JACS
JOURNAL OF THE AMERICAN CHEMICAL SOCIETY

ARTICLE

pubs.acs.org/JACS

Oxygen-Tolerant [NiFe]-Hydrogenases: The Individual and Collective Importance of Supernumerary Cysteines at the Proximal Fe-S Cluster

Michael J. Lukey,[†] Maxie M. Roessler,[†,‡] Alison Parkin,[†] Rhiannon M. Evans,[†] Rosalind A. Davies,[†] Oliver Lenz,[§] Baerbel Friedrich,[§] Frank Sargent,[∥] and Fraser A. Armstrong*[,†,‡]

[†]Department of Chemistry and [‡]Centre for Advanced Electron Spin Resonance, University of Oxford, South Parks Road, Oxford OX1 3QR, U.K.

[§]Department of Microbiology, Humboldt-Universität zu Berlin, Chausseestrasse 117, 10115 Berlin, Germany

[∥]College of Life Sciences, University of Dundee, Dow Street, Dundee DD1 5EH, U.K.

Supporting Information

ABSTRACT: An important clue to the mechanism for O_2 tolerance of certain [NiFe]-hydrogenases is the conserved presence of a modified environment around the iron−sulfur cluster that is proximal to the active site. The O_2-tolerant enzymes contain two cysteines, located at opposite ends of this cluster, which are glycines in their O_2-sensitive counterparts. The strong correlation highlights special importance for electron-transfer activity in the protection mechanism used to combat O_2. Site-directed mutagenesis has been carried out on *Escherichia coli* hydrogenase-1 to substitute these cysteines (C19 and C120) individually and collectively for glycines, and the effects of each replacement have been determined using protein film electrochemistry and electron paramagnetic resonance (EPR) spectroscopy. The "split" iron−sulfur cluster EPR signal thus far observed when oxygen-tolerant [NiFe]-hydrogenases are subjected to oxidizing potentials is found not to provide any simple, reliable correlation with oxygen tolerance. Oxygen tolerance is largely conferred by a single cysteine (C19), replacement of which by glycine removes the ability to function even in 1% O_2.

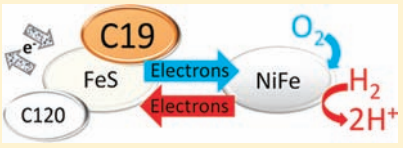

INTRODUCTION

Hydrogenases—microbial metalloenzymes that catalyze rapid H^+/H_2 interconversion—are usually regarded as very air-sensitive enzymes.[1] Consequently, any ability of hydrogenases to remain functional in the presence of O_2 is important because these enzymes, the organisms that host them, and inspired synthetic catalysts hold considerable promise for future H_2-energy technologies.[2−6] Typically, [NiFe]-hydrogenases consist minimally of a large subunit that houses the active site and a small subunit containing at least one electron-transferring Fe-S cluster: respiratory [NiFe]-hydrogenases contain three such Fe-S clusters that are proximal, medial, and distal to the active site and form a relay to the surface of the protein.[7] The active site (Figure 1) contains Ni and Fe with thiolates (four cysteines bound to Ni, two of which are bridging to the Fe), CO, and CN^- in a fragile, electron-rich environment that is a natural target for O_2. Indeed, "standard" [NiFe]-hydrogenases, which operate under anaerobic conditions *in vivo*, are inactivated by traces of O_2.[1,8−12] However, some [NiFe]-hydrogenases can exhibit high H_2 oxidation activity for sustained periods under aerobic conditions and are defined as "O_2-tolerant";[13] consequently, certain microorganisms, including pathogens, can utilize H_2 during aerobic growth.[1] Notable examples are some closely related membrane-bound [NiFe]-hydrogenases—from *Ralstonia eutropha* (*Re*-MBH),[13,14] from *Escherichia coli* (*Ec* Hyd-1),[15] from *Aquifex aeolicus* (*Aa* Hase I),[16,17] and from *Salmonella enterica* (Hyd-5),[18] all of which are currently subjects of intense research activity.[19−21]

A recent model[22] for O_2 tolerance of [NiFe]-hydrogenases stressed that the enzyme, upon attack by O_2, must immediately furnish all four electrons needed to avoid reactive oxygen species that damage or block the active site. Electron deficiency during O_2 attack results, at best, in the so-called "unready" state that is reactivated very slowly upon reduction.[8,12,23] During H_2 oxidation, O_2-tolerant hydrogenases survive O_2 by forming only the "ready" state, in which O_2 has been fully reduced, which reactivates very rapidly to rejoin the catalytic cycle.[22] As their names imply, "unready" and "ready" states are distinguished on the basis of their reactivation rates, but they have also been associated with spectroscopically defined states known respectively as Ni-A and Ni-B that are distinguished by electron paramagnetic resonance (EPR)[24] or infrared techniques.[25] It is widely recognized that there is a strong identity between "ready" and Ni-B, which is well characterized as a Ni(III) species having a OH^- ligand in the bridging position; in contrast, the relationship between "unready" and Ni-A is less clear, and there appear to be unready states without a spectroscopic connection with Ni-A, a particular case being [NiFeSe]-hydrogenases.[26,27] Proposals for the unready state(s) include forms having a peroxido ligand[12] and/or forms in which cysteines have been modified by O-atom attachment to S.[7,12,28,29] Other oxygenated inactive states may be more difficult to reactivate and more elusive spectroscopically;

Received: June 10, 2011
Published: September 15, 2011

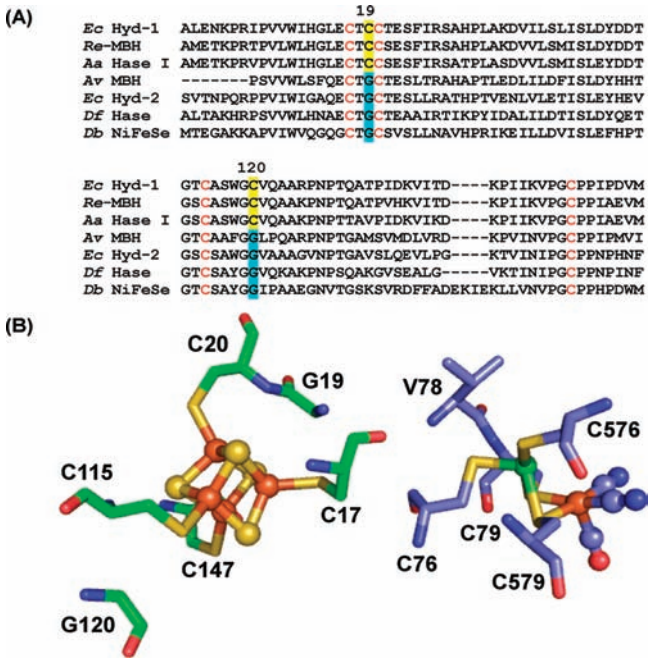

Figure 1. Multiple sequence alignment of key regions of the small subunits of a selection of [NiFe]-hydrogenases and the [NiFeSe]-hydrogenase from *Desulfomicrobium baculatum*, where *Ec* Hyd-1 = [NiFe]-hydrogenase 1 from *Escherichia coli*, *Re*-MBH = membrane-bound [NiFe]-hydrogenase from *Ralstonia eutropha*, *Aa* Hase I = [NiFe]-hydrogenase I from *Aquifex aeolicus*, *Av* MBH = [NiFe]-hydrogenase from *Allochromatium vinosum*, *Ec* Hyd-2 = [NiFe]-hydrogenase 2 from *E. coli*, *Df* Hase = [NiFe]-hydrogenase from *Desulfovibrio fructosovorans*, and *Db* NiFeSe = [NiFe-Se]-hydrogenase from *D. baculatum*. (A) The four cysteine residues known to coordinate the proximal cluster of *Df* Hase (C17, C20, C115, and C147 in *Ec* Hyd-1 numbering) are shown in red. The two supernumerary cysteine residues (C19 and C120 in *Ec* Hyd-1 numbering) that are found only in O_2-tolerant enzymes are highlighted in yellow, with the corresponding glycines in standard [NiFe]-hydrogenases and *Db* NiFe-Se highlighted in cyan. (B) The amino acid environment of the proximal [4Fe-4S] cluster in *Df* Hase (PDB: 1YRQ), with the residue numbering altered to reflect that of *Ec* Hyd-1. Small subunit residues have a green carbon backbone, while the Fe-S cluster is shown in stick-and-sphere representation. The [NiFe] active site is also shown with the Fe atom, its carbonyl ligands, and the Ni atom in a stick-and-sphere representation. Large subunit residues have a blue carbon backbone. The two terminal Ni-ligating cysteines (C76 and C576) and the Ni−Fe-bridging μ-cysteines (C79 and C579) are also shown.

for example, O_2 damage might be directed to an Fe-S cluster or to an active-site cysteine without accompanying formation of Ni(III). The active site cycles through various oxidation levels: as a guide, if O_2 attacks the active site when it is in the well-established state known as Ni-C (which is two electrons more reduced than Ni(III)), a further two electrons (as well as the proton requirement) must be provided very rapidly to complete its four-electron reduction to water.

Observations made for the *Re*-MBH, *Ec* Hyd-1, and *Aa* Hase I enzymes yield the following tentative list of characteristics shared by all O_2-tolerant hydrogenases: (1) avoidance of unready species during reaction with O_2 (as discussed above);[22] (2) resistance to CO,[15,20,30] a strong inhibitor of standard [NiFe]-hydrogenases;[10] (3) almost total catalytic bias toward H_2 oxidation vs H_2 evolution;[11,15,17] (4) fast, spontaneous activation of Ni-B under mildly reducing conditions at a characteristic potential known as E_{switch}[11,15,17,31] (noting that E_{switch}, which is measured under steady-state H_2 oxidation, is not equivalent to the midpoint potential measured by spectroscopy for the one-electron conversion of Ni-B to Ni_r-SI[24,31−33]); (5) an unusual EPR spectrum under oxidizing conditions, in which the signal of the $[3Fe\text{-}4S]^+$ medial cluster shows a multiline pattern due to coupling with a nearby paramagnetic site;[15,21,34] and finally, (6) O_2-tolerant membrane-bound hydrogenases contain two conserved cysteines that correspond to conserved glycines adjacent to the proximal [4Fe-4S] cluster in standard hydrogenases. This final point is discussed in more detail below and is the principal subject of this paper.

Efforts to elucidate the origins of O_2 tolerance in respiratory [NiFe]-hydrogenases have largely addressed the large subunit and have focused on how an O_2 molecule can be prevented from attacking the active site.[9,35−39] Investigations by site-directed mutagenesis have started either from an O_2-tolerant enzyme—altering residues and testing for a decrease in O_2 tolerance[19,38]—or from a standard hydrogenase—altering residues and looking for any increase in O_2 tolerance.[9,35−37,39] The most dramatic improvement to a standard hydrogenase achieved so far was reported recently by Liebgott et al.[39] as part of extensive studies of the [NiFe]-hydrogenase from *Desulfovibrio fructosovorans* (*Df* Hase).[9,35−37,39] Valine-74 of the large subunit (valine-78 in *Ec* Hyd-1, see Figure 1) is a fully conserved residue that occupies a position close to a bottleneck for gas molecule access to the active site, and changing it to a cysteine (a residue not found in this position in nature, either in standard or in O_2-tolerant [NiFe]-hydrogenases) resulted in a large increase in O_2 tolerance.[39] Compared to the native enzyme, the V74C variant recovered much more rapidly and completely after short pulses of O_2, was 20−25 times less sensitive to CO, and showed a value of E_{switch} after anaerobic inactivation that was midway between those for the native enzyme and the O_2-tolerant *Re*-MBH.[39]

Sequence alignments show that the differences between O_2-tolerant and standard hydrogenases are equally marked in large and small subunits. In particular (observation (6) of the above-mentioned list of tentative characteristics), O_2-tolerant membrane-bound hydrogenases contain two conserved cysteines (C19 and C120 in HyaA, the small subunit of *Ec* Hyd-1) that correspond to conserved glycines adjacent to the proximal [4Fe-4S] cluster in standard hydrogenases.[1,19,21,34] For reference, distances between the Ni and α-carbon atoms of the four proximal cysteines and V74 in *Df* Hase are included in the Supporting Information. Figure 1 shows that C19 replaces a glycine (in standard hydrogenases) lying between the proximal cluster and the active site, whereas C120 replaces a glycine that is located on the opposite side of the cluster. The presence of these supernumerary cysteines has suggested the possibility of a crucial role for the proximal cluster in conferring O_2 tolerance, and three recent papers have addressed this issue. Lenz and co-workers,[19] working on *Re*-MBH, described spectroscopic and functional comparisons between the native enzyme and a variant, C19G/C120G, in which both supernumerary cysteines were substituted by glycines. The C19G/C120G variant showed greatly diminished O_2 tolerance *in vivo* and *in vitro*, and the unusual spectral features at high potential (the complex multiline $[3Fe\text{-}4S]^+$ signal and coupling that alters the Ni-B spectrum) were abolished.[19] The second paper, by Lubitz and co-workers,[21] who studied *Aa* Hase I, specifically addressed the unusual EPR spectral features. By also applying Mössbauer spectroscopy, the authors proposed that the proximal cluster has unique coordination at one Fe subsite, possibly recruiting a second cysteine: they suggested

further that this feature might allow the cluster to perform not one but *two* sequential one-electron transfers—a property that should, as mentioned above, increase the rate and/or probability of delivering the rescue electrons to the active site when O_2 attacks.[21] Interestingly, [4Fe-4S] clusters are not otherwise known to perform multiple electron transfers without some rearrangement of the surrounding environment. The third paper, by Haumann and co-workers,[40] reports a comparison by X-ray spectroscopy of *Re*-MBH and the standard [NiFe]-hydrogenase from *Desulfovibrio gigas*. The data were interpreted in terms of the proximal cluster in *Re*-MBH consisting of a 3Fe unit and a more isolated Fe atom (Fe−Fe vectors ≥3.4 Å). These papers thus auspicate much clearer questions, regarding whether *either* or *both* of the supernumerary cysteines is responsible for O_2 tolerance and which of the observations (1)−(5) are linked to observation (6).

In this work, noting that *E. coli* should be particularly amenable to site-directed mutagenesis and capable of producing both O_2-tolerant and O_2-sensitive hydrogenases,[15,19] we have systematically exchanged C19 and C120 in the small subunit of *Ec* Hyd-1 for glycine. In order to determine the individual and collective roles of the cysteine residues in the characteristics (1)−(5) listed above, the enzymes Hyd-1 (native), C19G, C120G, and C19G/C120G were compared using conventional hydrogenase solution assays and the complementary techniques of protein film electrochemistry (PFE) and EPR spectroscopy. In PFE, tiny amounts of active enzyme are adsorbed directly onto an electrode surface.[10] Catalytic activity is directly controlled through the applied electrode potential and simultaneously monitored via the electrical current, while substrate and inhibitors are supplied at precise concentrations by varying the gas mixtures passing through the headspace of the electrochemical cell or by injecting directly into the cell solution. Catalytic current is directly proportional to the turnover frequency of active enzyme and its coverage density at the electrode surface. The technique greatly facilitates the study of reactions of hydrogenases with O_2, since soluble electron donors/acceptors that invariably react with O_2 are not required, and the status of the enzyme can be monitored over many hours, during which an extremely high number of turnovers may have occurred. EPR spectroscopy is the standard method for identifying Ni-A and Ni-B and various states of the Fe-S centers.[25] It is impossible to have exactly corresponding conditions for EPR and PFE experiments. The latter records steady-state activity, and thus only active enzyme is monitored, and a substrate must be present; in contrast, EPR samples are prepared by stoichiometric reactions or by titrating reducing or oxidizing agents into bulk solutions of enzyme (typically 10−100 μM) to achieve the desired solution equilibrium potential. In preparing an EPR sample of a hydrogenase, only a limited number of turnovers is possible, and true, potential-equilibrated samples of active enzyme in the presence of a high level of H_2 cannot be prepared at potentials more positive than −0.36 V (at pH 6) because almost all the available H_2 (concentration <1 mM at 1 atm, 25 °C—only a few times more than the enzyme concentration required for EPR) is consumed too quickly.

This study demonstrates that C120 does not play a critical role in the O_2, tolerance of *Ec* Hyd-1, but that substitution of C19 by glycine is sufficient to abrogate enzyme activity, even in the presence of only 1% O_2. The implications of this discovery and the accompanying EPR results are discussed with relation to the molecular mechanism of O_2 tolerance.

MATERIALS AND METHODS

Protein Film Electrochemistry. Protein film electrochemistry experiments were carried out in an anaerobic glovebox (Vacuum Atmospheres or M Braun) containing a N_2 atmosphere (O_2 < 2 ppm). Measurements were made using an electrochemical analyzer (Autolab PGSTAT128N) controlled by NOVA software (EcoChemie). The pyrolytic graphite "edge" (PGE) rotating disk electrode (geometric surface area 0.03 cm^2) was used in conjunction with an electrode rotator (EcoChemie or EG&G) in a sealed glass electrochemical cell. The three-electrode configuration was completed by a Pt wire counter electrode and a saturated calomel reference electrode (SCE), located in a side arm (25 °C) containing 0.10 M NaCl and separated from the main cell compartment by a Luggin capillary. Potentials (E) are quoted with respect to the standard hydrogen electrode (SHE) using the correction $E_{SHE} = E_{SCE} + 241$ mV at 25 °C.[41] All solutions were prepared using purified water (Millipore, 18 MΩ cm) and included a mixed buffer system[33] titrated to the desired pH at the experimental temperature. Experiments were performed under gas mixtures of H_2 (Premier grade, Air Products), CO (Air Products), Ar (BOC gases), and O_2 (BOC gases), controlled using precision mass flow controllers (Sierra Instruments).

To prepare an enzyme film, the PGE electrode was abraded with P400 Tufbak Durite sandpaper and then wiped with cotton wool. Enzyme solution (1 μL, 10−100 μM) was pipetted onto the surface and left for ∼30 s, and the surplus was rinsed off under a stream of purified water. The electrode was then placed in enzyme-free buffered electrolyte. The electrode was rotated at a constant rate (≥3000 rpm) to provide an efficient supply of substrate to and removal of product from the electrode surface. To activate the enzyme adsorbed on the electrode surface, a two-stage potential poise process was repeated until the enzyme was fully active: first, the potential was held at −0.56 V for 300 s, and then it was stepped to −0.06 V for 100 s. The activation took about 2 h and was judged to be complete when the H_2 oxidation current measured at −0.06 V no longer increased following reduction at −0.56 V.

Hydrogenase Solution Assays. The H_2 oxidation activity of native and variant Hyd-1 enzymes (0.5−15 μg) was determined using a conventional solution assay.[42] Benzyl viologen (BV, 50 mM in hydrogen-saturated mixed buffer solution at pH 6[33]) was used as the electron acceptor under 100% H_2 at 25 °C. A Perkin-Elmer Lambda 19 spectrophotometer was used to monitor the change in absorbance with time at 600 nm as BV was reduced by the electrons produced from H_2 oxidation. The enzyme activity, expressed in μmol H_2 min^{-1} mg^{-1}, was determined using an extinction coefficient for BV of 7.4 cm^{-1} mM^{-1}.[43] Protein concentrations were estimated spectroscopically using the method of Bradford.[44]

Electron Paramagnetic Resonance (EPR) Spectroscopy. Samples at defined potentials for EPR measurements were prepared as follows: Native or variant enzymes in 0.10 M MES, 0.10 M NaCl, pH 6, at 20 °C, 10% glycerol were transferred to an Ar-purged "titration cell", similar to that first described by Dutton.[45] A two-electrode system was used to determine the equilibrium solution potential. The working electrode was the platinum ring of a combination electrode (Mettler Toledo, InLab Redox Micro), and the reference electrode was a micro Ag/AgCl electrode (WPI, DRIREF-2). Potentials are quoted with respect to SHE using the correction $E_{SHE} = E_{Ag/AgCl} + 195$ mV at 20 °C (calibrated with quinhydrone (Aldrich) at pH 4 and 7). Argon and H_2 gases were passed through an O_2 scrubber (Gas Clean Filters, Varian) before entering the titration cell, and a stirrer bar ensured constant mixing of the enzyme solution. For precise temperature control, the cell was water jacketed, and to avoid inward leakage of atmospheric O_2, it was kept under positive gas pressure. This also allowed EPR samples to be withdrawn by transferring ∼150 or ∼300 μL

of enzyme solution from the cell through a stainless steel outlet tube into an EPR tube that had been previously purged with the gas mixture of the cell. The sample was then flash-frozen in an isopropanol slush (isopropanol stirred over liquid N_2).

To make the enzyme samples measured for the spectra shown in Figure 7, bulk "as-isolated" hydrogenase samples were first activated under 100% H_2 at 37 °C with an initial injection of 0.4−0.6 μL of 0.40 M sodium dithionite (Sigma Aldrich) and redox mediators (methyl viologen, benzyl viologen, phenazinemethosulfate, indigotetrasulfonate, 1,2-naphthoquinone, and 2-hydroxyl-1,4-naphthoquinone, 40 μM each). After equilibration to the $2H^+/H_2$ potential, half of the H_2-saturated enzyme was frozen for subsequent aerobic inactivation, and the other half was anaerobically inactivated: after flushing out the H_2 with Ar at 30 °C, the temperature was returned to 20 °C, the potential was raised to +78 ± 2 mV by adding a substoichiometric amount of potassium ferricyanide (Sigma Aldrich), and the sample was withdrawn and frozen. The anaerobically inactivated native Hyd-1 sample (∼300 μL, sufficient to fill the resonator height) was transferred to a high-precision EPR tube (Wilmad, 714-PQ-7) for accurate spin quantification (Figure 7A); all other samples were transferred to standard tubes. The aliquot of enzyme taken for aerobic inactivation was defrosted under the titration cell atmosphere and returned to the cell. The enzyme was exposed to 10% O_2 in Ar (total flow rate 100 (standard cubic centimeters) min^{-1}) at 30 °C for 4000 s, O_2 was flushed out of the cell with Ar until the potential was steady, the temperature was then returned to 20 °C, the potential was adjusted to +77 ± 2 mV under Ar by adding sodium dithionite, and the sample was withdrawn and frozen.

To make the enzyme samples measured for the spectra shown in Figure 8, as-isolated hydrogenase containing the same cocktail of redox mediators as above was titrated to the desired potential under Ar, and samples were withdrawn (∼300 μL, sufficient to fill the resonator height) into high-precision EPR tubes (Wilmad, 714-PQ-7) for analysis. The enzyme concentration of samples at different potentials is essentially constant because only very tiny amounts of oxidizing and reducing agents (ferricyanide and dithionite) were added. Samples were taken in the following order: native Hyd-1 (+145, +265, +385, +175 mV), C120G (+147, +265, +387, +326 mV), C19G/C120G (+241, +393, +148 mV), and C19G (+145, +264, +384 mV).

Continuous-wave (CW) EPR experiments were performed using an X-band (9−10 GHz) Bruker EMX spectrometer (Bruker BioSpin GmbH, Germany) with an X-band super-high-sensitivity probehead (Bruker) equipped with a low-temperature helium flow cryostat (Oxford Instruments CF935). For determining g values, the magnetic field was calibrated at room temperature with 2,2-diphenyl-1-picrylhydrazyl as external standard (g = 2.0036). A background spectrum was recorded under identical conditions and subtracted from the EPR spectrum of the enzyme sample. Data analysis was performed using the program EasySpin.[46]

Spin quantification was carried out using a calibration line obtained with copper perchlorate samples (20, 50, 100, 150, and 200 μM $CuSO_4$ in 2 M $NaClO_4$(aq) adjusted to pH 1.22 with HCl) measured under nonsaturating conditions.

Preparation of Hydrogenases. The *E. coli* K-12 strains used for protein expression in this study were FTH004,[47] ML23, ML24, and ML25, all of which are derived from MC4100.[48] All strains carry an engineered *hyaABCDEF* operon encoding a modified HyaA protein (Hyd-1 small subunit) bearing a His_6 affinity tag at the extreme C-terminus. Hyd-1 enzyme produced from strain FTH004 is hereafter referred to as "native" Hyd-1. In strain ML23, *hyaA* is further modified to encode a C19G/C120G double-exchange HyaA protein (referred to as C19G/C120G), strain ML24 encodes a C120G HyaA protein (referred to as C120G), and strain ML25 encodes a C19G HyaA protein (referred to as C19G). The construction of mutant strains is described in the Supporting Information. *E. coli* strains FTH004, ML23, ML24, and ML25 produce His-tagged native and variant Hyd-1 enzymes under normal physiological regulatory and biosynthetic control. Isolation of native Hyd-1 and all three variants was carried out as described previously.[15] For optimal expression of the *hya* operon and subsequent production of the Hyd-1 enzymes, each strain was cultured anaerobically. The rate of growth and final cell density were similar for each strain. The yield of hydrogenase was ∼0.15 mg (g of cells)$^{-1}$ from strains FTH004, ML23, and ML25 and was 2−3 times lower from strain ML24. Purified native Hyd-1 from strain FTH004 was indistinguishable by SDS-PAGE from all other variants, as shown in Figure S1.

Several lines of evidence showed that all variants and native enzyme contain a full complement of cofactors, as required for catalytic competency. All enzymes were isolated from the membrane fraction, indicating that these hydrogenases must be correctly assembled and folded since their targeting to the membrane requires the twin arginine translocation (Tat) system, which will systematically reject immature or misfolded proteins. Samples for which the metal contents were quantified by total-reflection X-ray fluorescence analysis (Michael Haumann, personal communication) showed the following Fe/Ni ratios: native Hyd-1, 11.0 ± 0.3; C19G, 12.1 ± 0.5; and C120G, 12.6 ± 0.5 (C19G/C120G was not measured). All four enzymes showed high catalytic activities in anaerobic electrochemical experiments (see below): conventional solution assays using 50 mM BV as electron acceptor (i.e., under small driving force conditions) gave (μmol H_2 min^{-1} mg^{-1}) native Hyd-1, 59 ± 3; C19G/C120G, 29 ± 3; C19G, 15 ± 1; and C120G, 41 ± 1.

RESULTS

The cyclic voltammograms shown in Figure 2 reveal how each of the fully activated hydrogenases responds to a *transient* burst of O_2. As the potential was raised from −0.43 to +0.24 V at 0.5 mV s^{-1}, O_2-saturated buffer was injected into the cell solution under mildly oxidizing conditions (+0.03 V, a potential at which anaerobic inactivation is not significant; see later discussion of E_{switch}) to give a total concentration of 0.16 mM. Continuous flow of H_2 through the headspace ensured that almost all O_2 was flushed from solution before the scan direction was reversed ($t_{1/2}$ ≈ 1 min). Following the O_2 burst, only native Hyd-1 recovers activity during the scan to high potential (the forward scan); likewise, on the *reverse scan* (as measured at −0.10 V) only the native enzyme has recovered the initial activity recorded during the forward scan. On the basis of the difference in current between the forward and reverse scans at −0.10 V (as depicted by the depth of the horizontal gray strip in Figure 2), it is established that tolerance to short-term O_2 exposure decreases in the order Hyd-1 > C120G > C19G/C120G > C19G. All enzymes show negligible H^+ reduction activity and an identical overpotential requirement for the onset of H_2 oxidation.

The effect of *prolonged* O_2 exposure on the H_2 oxidation activity of each enzyme is displayed in Figure 3. Additionally, the effect of altering the potential at which O_2 is introduced, 0 V compared to −0.10 V, was investigated—the lower potential providing a stronger external driving force to (a) supply electrons at the time of O_2 attack and (b) reactivate Ni-B. The level of H_2 was decreased from 100% to 10%, and then the concentration of O_2 was varied while the H_2 concentration was maintained at 10%. The current traces measured at 0 V for both native Hyd-1 and C120G under 1% O_2 (vertical dotted blue line) reach a constant plateau at a significant current reading, thus showing that H_2 oxidation is sustainable in the presence of O_2. This tolerance is in striking contrast to the C19G/C120G and C19G variants, for which introduction of just 1% O_2 into the cell headspace results in a continuous decrease in current until it eventually reaches a

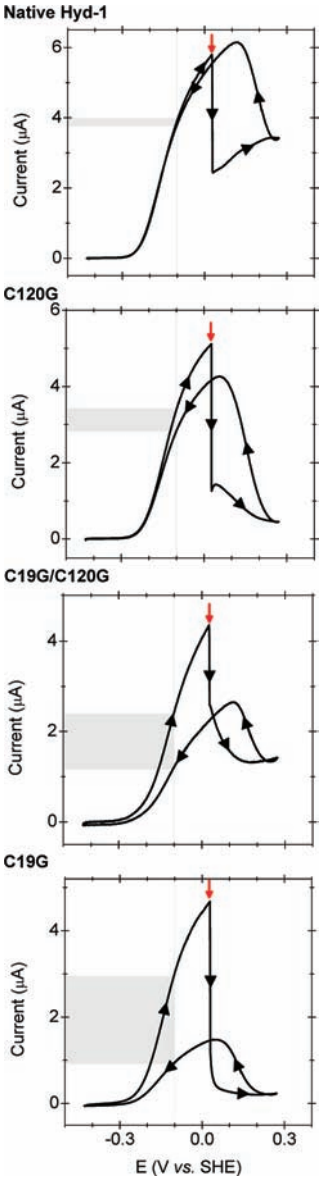

Figure 2. Contrasting effects of a brief exposure to O_2 on the H_2 oxidation activities of native and variant Hyd-1 enzymes. Cyclic voltammograms were recorded under a headgas atmosphere of 100% H_2 (gas flow rate 1000 (standard cubic centimeters) min^{-1}) at pH 6.0, 30 °C, scan rate 0.5 mV s^{-1}. Black arrows indicate the direction of the potential sweep. A red arrow indicates the point of injection of O_2-saturated buffer into the cell solution at +0.03 V on the forward scan, to give an O_2 concentration of 0.16 mM. The O_2 concentration immediately begins to fall due to continued flushing with H_2, and by the time a potential of +0.25 V is reached and the scan direction reverses, almost all O_2 has been flushed from solution. A horizontal gray strip indicates the difference in current recorded at a potential of −0.10 V on the forward and reverse scans. All enzymes show negligible H_2 evolution activity and a marked overpotential requirement for H_2 oxidation.

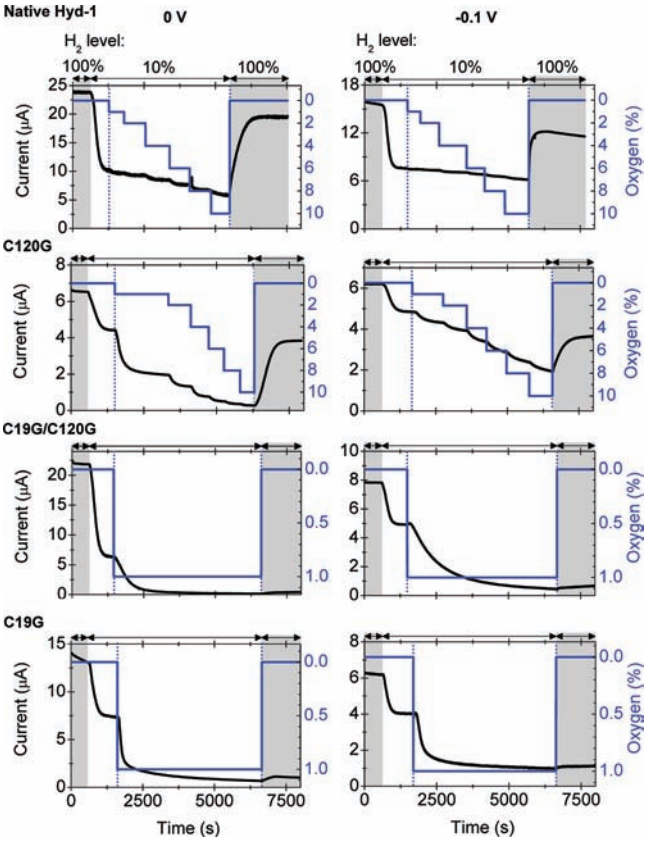

Figure 3. Current−time traces recorded at 0 (left) and −0.1 V (right), at pH 6, 30 °C, under a variable controlled H_2/O_2 headgas atmosphere with Ar as carrier gas (gas flow rate 1000 (standard cubic centimeters) min^{-1}). The O_2 concentration in is shown in blue, and the recorded currents are shown in black. Immediately prior to O_2 exposure, currents were recorded at 100% and 10% H_2, and following exposure of each enzyme to O_2, anaerobicity was restored to 100%, as indicated by gray boxes. Hydrogen composition during O_2 exposure remained at 10%, as labeled in the upper-most panels.

negligible value. The corresponding experiments conducted at −0.10 V showed that all enzymes have increased O_2 tolerance at this more negative potential but with relative differences: C120G shows approximately twice the inhibition experienced by native Hyd-1. Although neither the C19G nor the C19G/C120G protein is capable of sustained catalysis of H_2 oxidation in the presence of 1% O_2, C19G is inactivated much more rapidly than C19G/C120G after the introduction of 1% O_2 into the headspace. The experiments thus establish that tolerance to more prolonged O_2 exposure lies in the order Hyd-1 > C120G ≫ C19G/C120G ∼ C19G; i.e., there are clearly two classes of enzyme, with C120G resembling the native enzyme in having a high degree of O_2 tolerance, and C19G and C19G/C120G resembling standard hydrogenases in having little O_2 tolerance.

The level of *spontaneous* recovery (i.e., without requiring application of a more negative potential) from O_2 inactivation is estimated by returning the headspace atmosphere to 100% H_2 and comparing the resulting current with that measured before O_2 was introduced. The native Hyd-1 and C120G enzymes show significant recovery under these conditions, whereas the C19G/C120G and C19G variants show very little. These experiments, conducted over long periods of time, are complicated by slow, irreversible activity loss unrelated to reaction with O_2.

Importantly, the potentials used in the experiments in Figure 3 were not effective in driving spontaneous recovery of aerobically generated states in the case of C19G/C120G and C19G. This observation was probed further by cyclic voltammetry (CV) (Figure 4) and potential-step chronoamperometry (Figure 5) to determine if catalytic activity could be recovered at a more

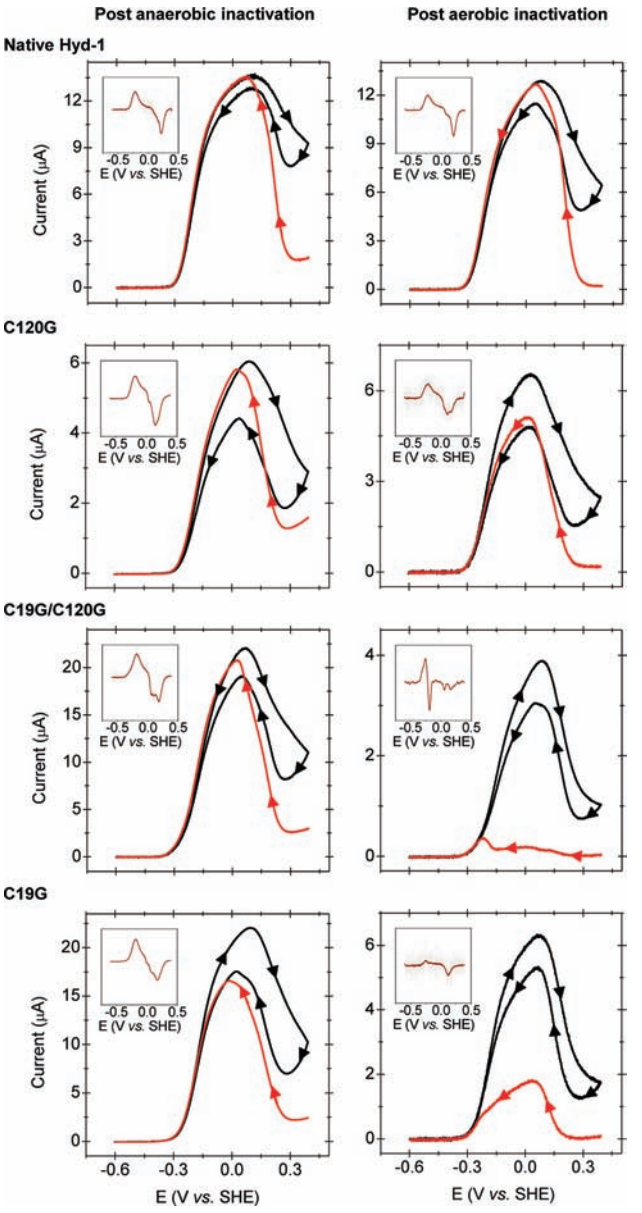

Figure 4. Cyclic voltammograms showing reactivation of the anaerobically generated (left) and aerobically generated (right) inactive states. The insets show the derivative plots of the red traces. The scans were recorded under a headgas atmosphere of 100% H_2 at pH 6.0, 30 °C, scan rate 0.1 mV s^{-1}. The anaerobic inactivation protocol was a potential poise at +0.39 V for 10 000 s (see Figure S3A), immediately followed by the reactivation potential sweep from +0.39 to −0.6 V (red trace). A second potential sweep was immediately initiated (black trace) to evaluate how much enzyme activity was recovered during the first sweep to low potential. The aerobic inactivation protocol (see Figure S3B) was as follows: the electrode potential was first poised at 0 V with a gas flow of 10% H_2 for 600 s, and the atmosphere was changed to 10% O_2, 10% H_2 for 2000 s. At 2600 s, the electrode potential was raised to +0.39 V, and at 3200 s, the gas flow was changed back to 100% H_2 for 1000 s to flush O_2 from the cell prior to the potential sweep from +0.39 to −0.6 V (red trace). This potential sweep was immediately continued (black trace) to evaluate how much activity was recovered during the first sweep to low potential. Arrows indicate the direction of the potential sweep. The total gas flow rate for all experiments was 300 (standard cubic centimeters) min^{-1}.

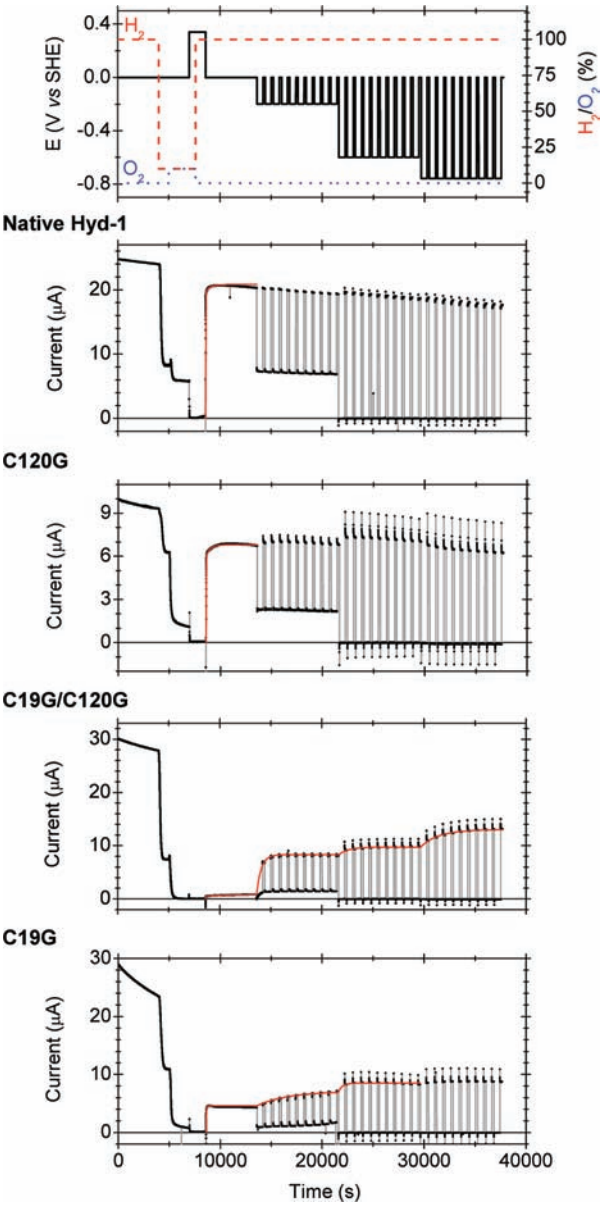

Figure 5. Current−time traces to monitor the inhibition and subsequent requirement for low potential steps to drive reactivation of enzyme exposed to 10% O_2 in 10% H_2 with Ar as carrier gas at pH 6.0, 30 °C. The electrode potential was first poised at 0 V to allow monitoring of initial activity in 100% H_2 for 4000 s. This potential was maintained throughout the gas equilibration stages. From 4000 to 5000 s, 10% H_2 was flowed through the cell, and then from 5000 to 7000 s, the gas was 10% O_2, 10% H_2. At 7000 s, the electrode potential was raised to +0.39 V, and at 7600 s, the gas flow was changed back to 100% H_2 for the remainder of the experiment. At 8600 s, the potential was returned to 0 V, and reactivation at this potential was monitored for 5000 s. A series of steps to lower potential followed by a return to 0 V (see black trace in top panel) were applied to assess the requirement for low-potential activation of aerobically generated states. For clarity, the red lines denote exponential fits to current measured at 0 V. Gas changes are also indicated on the top panel, where the red trace indicates H_2 level and the blue trace indicates O_2 level. The total gas flow rate for all experiments was 300 (standard cubic centimeters) min^{-1}.

negative potential. The cyclic voltammograms were measured after either anaerobic inactivation, brought about by poising the electrode potential at +0.39 V for 10 000 s under 100% H_2 (Figure 4, left), or aerobic inactivation, brought about by

exposure to 10% O_2 (2000 s at 0 V, then 600 s at +0.39 V), followed by flushing of O_2 with H_2 (1000 s at +0.39 V) (Figure 4, right). Details of the inactivation procedures are given in Supporting Information, Figure S3. In each case, the voltammogram, recorded under 100% H_2 at a very slow scan rate (0.1 mV s^{-1}), starts with a reductive scan from +0.39 to −0.60 V and is followed by a complete cycle from low potential to high potential and back again. After anaerobic inactivation, all variants showed full recovery of activity at 0 V on the initial reductive scan, and the minima in the derivative of the first reductive scans (see insets in Figure 4) give E_{switch} values as follow: Hyd-1, +0.21 V; C120G, +0.14 V; C19G/C120G, +0.18 V; and C19G, +0.17 V, all ±0.02 V. Therefore, in each case, reactivation of Ni-B occurs at high potential and is spontaneous at 0 V.

Following aerobic inactivation, both native Hyd-1 and C120G undergo only a single reactivation process at a high potential (around +150 mV) that is equal or very close to that measured after anaerobic inactivation. In contrast, for C19G/C120G and C19G, much less recovery occurs at high potential. For C19G, there is some recovery at high potential, but most reactivation occurs only after the potential has been taken to a value that is too negative to oxidize H_2; the extent of this low-potential reactivation is revealed after the scan direction is reversed. In the case of C19G/C120G, *barely any* reactivation occurs until the potential is taken below −0.20 V on the initial reductive sweep (this is clearly visible as a current increase at a potential slightly more positive than the onset potential of H_2 oxidation). Therefore, prolonged O_2 exposure causes C19G/C120G and C19G (but not native Hyd-1 or, to any degree, C120G) to accumulate states that are reactivated only upon application of strongly reducing conditions.

The rate−potential profiles of reactivation for all enzymes were investigated further by potential-step experiments, as shown in Figure 5. After inactivation by 10% O_2 in 10% H_2 (2000 s at 0 V, followed by 600 s at +0.39 V, i.e., as for Figure 4), the atmosphere was restored to 100% H_2, and then the potential was stepped to values more negative than E_{switch} to drive reductive reactivation. Upon stepping the electrode potential from +0.39 to 0 V, native Hyd-1 and the C120G variant show >90% and >75% recovery, respectively; the recovery is complete within several seconds, with little further increase after 5000 s. Subsequently stepping the potential to −0.20 and then to −0.60 V (see top panel of Figure 5) produces very little further increase in activity (as measured at 0 V) for native Hyd-1 and approximately 10% at both stages for C120G. In contrast, for C19G/C120G and C19G, significant reactivation is only achieved by stepping the potential to −0.20, −0.60, and −0.76 V. These results parallel the observations made by CV (Figure 4) and confirm that O_2 attacks C19G/C120G and C19G to give products that are reactivated *only* under much more extreme reducing conditions—consequently, these products accumulate upon prolonged O_2 exposure. The agreement between Figures 4 and 5 is noteworthy—even the slightly higher amount of spontaneous recovery seen (Figure 5) with C19G compared to C19G/C120G is consistent with the respective potential dependences of recovery shown in Figure 4.

To establish that variations in O_2 sensitivity do not arise from restricted access or binding of small gas molecules at the active site, experiments were performed to compare CO inhibition for the four enzymes. Carbon monoxide is a known competitive inhibitor of hydrogenases and should be an excellent probe of relative gas access and binding at the active site.[15] Relative to native Hyd-1, the variants showed only very small changes in CO sensitivity (Figure 6) and in no case approached the high degree of sensitivity displayed by standard hydrogenases such as *E. coli* Hyd-2 (see Figure S4).

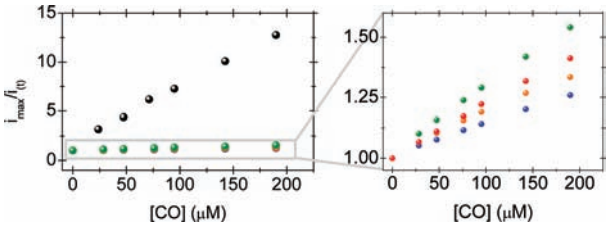

Figure 6. Comparative analysis of the CO sensitivity of the native Hyd-1 (red spheres), native Hyd-2 (black spheres), C120G (blue spheres), C19G/C120G (green spheres), and C19G (orange spheres) Hyd-1 variants. Data were extracted from current−time traces recorded at pH 6.0, 30 °C (see Figure S4). A constant headgas atmosphere of 20% H_2 was used, and the concentration of CO increased stepwise from 0% to 20%, with Ar as the carrier gas. The total gas flow rate was 500 (standard cubic centimeters) min^{-1}.

The results of EPR studies of native and variant Hyd-1 following either anaerobic or aerobic inactivation are shown in Figure 7. Spectra of as-isolated enzyme samples (see Figure S7 and ref 15) showed both Ni-A and Ni-B states, so it was necessary to ensure complete activation before O_2 experiments were carried out. The activation was carried out under 100% H_2 at 37 °C and deemed complete when the potential reached a steady value and when no more Ni-A signal was observed after raising the potential anaerobically (see Materials and Methods). Activation of native Hyd-1 required 4 h, C120G required 8 h, and C19G required 27 h. The C19G/C120G variant was very slow to activate; as shown in Figure 7A, the sample treated with H_2 for 24 h still shows Ni-A, and residual amounts of this state were only removed after 40 h. Similarly, shorter activation times for native Hyd-1 and the C19G and C120G variant enzymes showed that Ni-A was still present (not shown). The activation times for solution samples placed under H_2 (with no direct source of electrons) are much longer than observed for electrochemical activation under H_2.[8,23,49] Nonetheless, the long activation time required for the Hyd-1 enzymes is highly unusual compared to standard hydrogenases, which usually require between 1 and 2 h of activation. Indeed, the standard *E. coli* Hyd-2 hydrogenase is fully activated after 1 h under 100% H_2 at room temperature (data not shown).

The EPR spectra of activated native Hyd-1 show signals of reduced [4Fe-4S] cluster(s) very similar to those observed for *Aa* Hase I and *Re*-MBH (Figure S5).[15−17,19−21,34] Samples from several different preparations show that these Fe-S cluster signals integrate to 1.0 ± 0.2 spin per molecule.[50] For comparison, Saggu et al. have reported a value of 0.5−0.8 spin per molecule for *Re*-MBH.[34] However, as was also the case for the C19G/C120G variant from *Re*-MBH,[19] *no* signals were observed in this field range from any of the three activated variants (Figure S5), and we are currently investigating the possibility that the variants have reduced [4Fe-4S] cluster(s) with ground states that are not $S = 1/2$. Electrochemical measurements of aliquots of enzyme used to make the activated EPR samples of native Hyd-1 and the three variants showed similar high activity, and we therefore conclude that the Fe-S clusters are correctly assembled in all four enzymes. No significant amounts of Ni signals are observed at this potential in any of the four enzymes, in accord with what

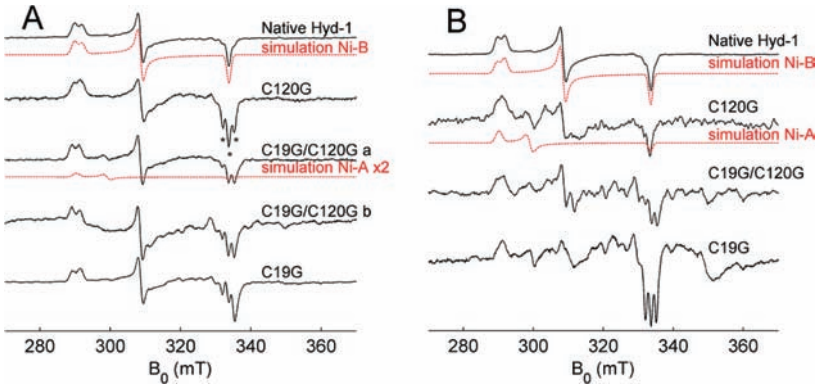

Figure 7. Comparison of the 9.39 GHz CW EPR spectra at 80 K of Hyd-1 and variant enzyme samples after H_2 reduction followed by either anaerobic inactivation (A) or aerobic inactivation (B), at +77 ± 2 mV. Prior to inactivation, samples were activated under H_2 for 4 h (native Hyd-1), 8 h (C120G), 27 h (C19G), 24 h (C19G/C120G a), and 40 h (C19G/C120G b). The simulation of the spectrum of the anaerobically inactivated native Hyd-1 is shown in red (Ni-B_1, $g_{x,y,z}$ = 2.314, 2.174, 2.010; Ni-B_2, $g_{x,y,z}$ = 2.297, 2.172, 2.010). *g*-values of the Ni-B species are comparable for the three variant enzymes. The C19G/C120G b spectrum shows a small amount of Ni-A (simulation of Ni-A shown in red, $g_{x,y,z}$ = 2.31, 2.24, 2.01). See Materials and Methods for details on sample preparation. Protein concentrations: native Hyd-1 (panel A), 57.3 μM; other sample concentrations were between 50 and 60 μM. Spectra were recorded with 2 mW microwave power and 1 mT modulation amplitude at 100 kHz. The resonator background (measured under identical conditions) was subtracted. Unidentified peaks are marked with an asterisk.

Goris et al. have reported for native *Re*-MBH and the C19G/C120G variant.[19]

After activation and anaerobic inactivation (equilibration of the potential to +78 mV), all enzymes showed clear Ni-B signals at 80 K (Figure 7A). Two Ni-B species with different g_x values (2.314 and 2.297) but identical g_y and g_z values are formed in all variants. The g_x peaks are unlikely to arise from a single species coupling to Fe-S centers since the latter are not detected at 80 K. The potential (+78 mV) was also carefully chosen such that a minimal number of Fe-S clusters are EPR active. The two different g_x values are consistently observed for samples following activation and anaerobic inactivation. At present, we do not understand the reason for this observation. However, it is interesting that these spectra also reveal a much more homogeneous sample compared to the as-isolated enzyme EPR spectra, in which only one g_x value is apparent (see Figure S7 for spectra of as-isolated enzyme samples, as well as ref 15 for native Hyd-1) and which show many peaks in addition to those for Ni-A and Ni-B.

A simulation for the Ni-B spectrum (red) of native Hyd-1 is shown. For native Hyd-1, the Ni-B signals amount to 0.6 ± 0.2 spin per molecule of enzyme. However, this value is an underestimate because titrations show that Ni-B is not fully formed at this potential. Higher potentials could not be used to maximize the intensity of the Ni-B spectrum because Ni-B experiences enhanced relaxation as the high-potential proximal center becomes oxidized, as discussed below. Although a precise quantification of the Ni signals was only carried out for native Hyd-1, the values for the variants must be similar, because similar enzyme concentrations were used and signal-to-noise ratios are comparable (Figure 7A).

Unidentified peaks are visible in all enzyme samples after H_2 treatment followed by anaerobic oxidation (marked in Figure 7A as * in the C120G spectrum). These peaks are also observed in *Aa* Hase I[21] and *Re*-MBH[34] and may be associated with degradation of the enzyme. However, the Fe-S clusters are unlikely to be damaged, as there was essentially no $g \approx 4.3$ signal corresponding to the presence of free Fe^{3+} which would originate from cluster deterioration (see wide-field spectra of anaerobically and aerobically inactivated C19G/C120G variant in Figure S6).

Figure 7B shows the 80 K EPR spectra of native Hyd-1 and proximal cluster variants after exposure of activated enzyme to O_2. Native Hyd-1 shows a spectrum almost identical to that obtained from the anaerobically inactivated sample in Figure 7A, with similarly good signal-to-noise ratio and thus comparable spin concentration, consisting solely of Ni-B. In contrast, a qualitative assessment of g_y signals shows that samples of the C120G, C19G/C120G, and C19G variants contain both Ni-A and Ni-B states. Despite enzyme concentrations similar to the native enzyme, the signal-to-noise ratio is much lower, suggesting strongly that the variant enzyme samples, particularly C19G and C19G/C120G, also contain EPR-silent states. Importantly, these spectra show that, on the basis of EPR alone, it is difficult to differentiate among the O_2 sensitivities of the different variants.

Quantitative assessment of the Ni-A:Ni-B ratio in Figure 7B was complicated by two factors. First, precise potential control during aerobic inactivation of the EPR enzyme samples is not possible, and previous electrochemical studies of [NiFe]-hydrogenase from *Allochromatium vinosum* showed that formation of Ni-A is potential dependent.[8,34] Second, additional peaks (e.g., those marked *) and broadened peaks prevented an accurate simulation of the spectra obtained after prolonged aerobic inactivation, and amounts could not be reliably assessed using only the g_y signal.

To investigate the correlation between the multiline EPR spectrum observed under oxidizing conditions and O_2 tolerance, as-isolated samples of the four enzymes were poised at a range of high potentials (+145 to +393 mV), and spectra were recorded at 15 K, at which temperature the $g = 2$ region is dominated by the medial $[3Fe\text{-}4S]^+$ cluster signal (Figure 8). Only the C19G/C120G variant exhibits a simple signal arising from the $[3Fe\text{-}4S]^+$ cluster at all potentials. The intensity of the signal grows with increasing potential, and at +393 mV the signal is at its maximum intensity and integrates to 0.9 ± 0.2 spin per molecule of enzyme. In native Hyd-1, a simple $[3Fe\text{-}4S]^+$ signal is only observed at moderately high potentials (+145 mV), and this changes, upon further oxidation, into the more complex signals that are also

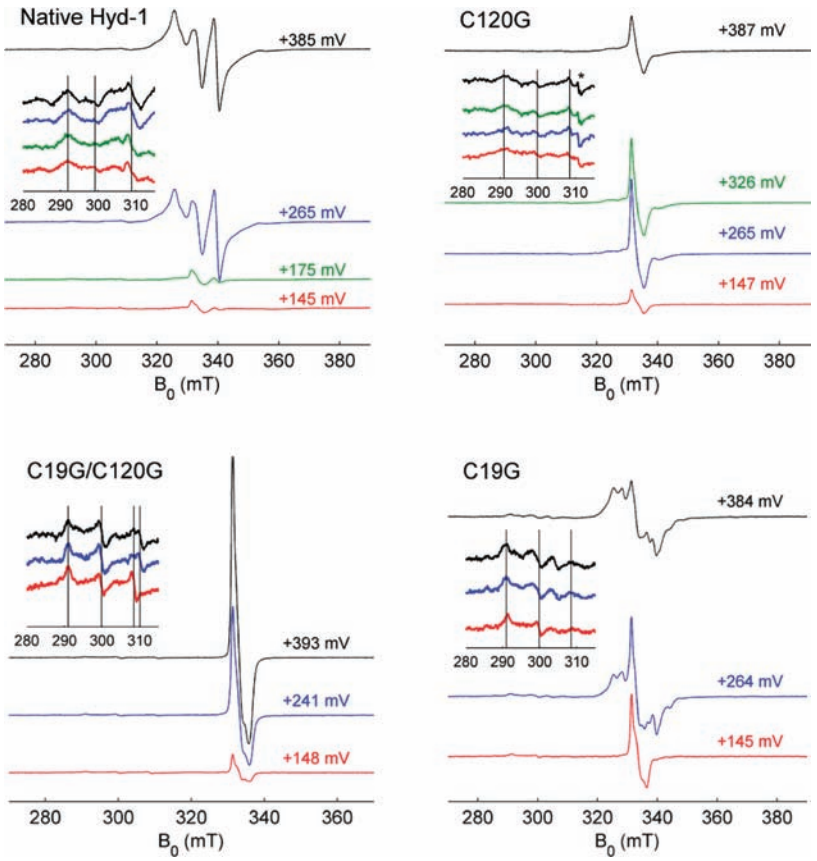

Figure 8. Comparison of the 9.39 GHz CW EPR spectra at 15 K of Hyd-1 and variant as-isolated enzyme samples poised at high potentials. Insets show a magnification of the Ni region of the spectrum. Vertical lines indicate the average *g*-values of Ni-A/Ni-B g_x, Ni-A g_y, Ni-B g_y (from left to right). The fourth line in the C19G/C120G spectrum represents the shift in Ni-B g_y consistently observed (see text). The signal observed at $g = 2.15$ in the C120G variant is unlikely to arise from Ni-B and is marked with an asterisk (see text). Approximate protein concentrations: 24 (native), 14 (C120G), 21 (C19G/C120G), and 16 μM (C19G). Spectra were recorded with 2 mW microwave power and 1 (native) or 0.5 mT (C19G, C19G/C120G, C120G) modulation amplitude at 100 kHz. The resonator background (measured under identical conditions) was subtracted. Ni signals are saturated at 2 mW microwave power to different extents depending on the enzyme (see text).

observed for the O_2-tolerant hydrogenases *Re*-MBH and *Aa* Hase I.[17−20] Double integration of the Fe-S cluster signals at +385 mV yielded 2.0 ± 0.3 spins per molecule of enzyme. A complex signal also forms in the C19G variant at high potentials (accounting for 2.1 ± 0.3 spins per molecule of enzyme), although it differs from that observed in the native enzyme. The midpoint potentials of the high-potential center and the $[3Fe\text{-}4S]^{+/0}$ transition observed in native Hyd-1 and the C19G variant are different: in native Hyd-1, the similarity in midpoint potentials makes it difficult to observe a spectrum due to uncoupled $[3Fe\text{-}4S]^{+}$, whereas for the C19G variant, a signal due solely to $[3Fe\text{-}4S]^{+}$ is clearly defined at +145 mV (pH 6). In the case of the C120G variant, the signal intensity of the $[3Fe\text{-}4S]^{+}$ cluster signal decreases with increasing potential, and the "wings" broaden. At +387 mV, the double integral of the Fe-S cluster signals amounts to 0.7 ± 0.3 spin per molecule of enzyme, i.e., more like the C19G/C120G variant. These spectral observations were fully reproducible over a range of samples from different enzyme preparations.

Insight into whether the Ni(III) center of the active site couples to the high-potential paramagnetic species is gained by inspecting the effect of potential on the Ni signals at low temperatures (insets in Figure 8). Black lines show the positions of the g_x components of Ni-A and Ni-B (average), g_y of Ni-A, and g_y from Ni-B. In the complete absence of a high-potential center (as in the C19G/C120G variant), no significant change is seen in the Ni region of the spectrum as the potential is increased. It is interesting to note that the Ni-B g_y peak sharpens and shifts from 2.161 to 2.173 upon reduction and anaerobic reoxidation. Because no shifts are observed for other redox-active species in the potentiometric titration, the shift in Ni-B g_y cannot be attributed to hysteresis. The Ni signals of native Hyd-1 and the C19G variant change with potential as the signal from the high-potential paramagnetic center appears (a change was difficult to ascertain for C120G). At 80 K, the Ni signals in these two enzymes are not observed at high potentials—a manifestation of the change in the relaxation properties of the Ni species, as also reported for *Aa* Hase I.[20] Accordingly, at 15 K, the Ni signals for C19G/C120G became saturated at much lower microwave power (≤0.008 mW) than for native Hyd-1 and the C19G variant (≤0.12 mW). The signal observed at $g = 2.15$ in the C120G variant (marked as * in the inset) is unlikely to arise from Ni-B, as it was also present in samples at lower potentials at which Ni-B and Ni-A are reduced (as judged by the absence of their characteristic g_x and g_y peaks).

DISCUSSION

The ability of *Ec* Hyd-1 to catalyze H_2 oxidation in the presence of O_2 depends crucially on the presence of a "supernumerary"

cysteine at position 19 in the small subunit and to a lesser extent on the co-presence of a second cysteine at position 120. When exposed to O_2 for a prolonged period during H_2 oxidation, native Hyd-1 produces only the ready state (which reactivates rapidly and spontaneously at relatively high potential), as measured by PFE; accordingly, the EPR spectrum obtained following exposure of activated native Hyd-1 to O_2 for 1 h, without H_2, shows only Ni-B. Replacing C120 with glycine results in an enzyme that can still function in the presence of O_2 for prolonged periods: however, states accumulate (around 10% after 1 h) that do not reactivate spontaneously, and the EPR spectrum of C120G after exposure to O_2 shows that some Ni-A is formed in addition to Ni-B.

In contrast, replacement of C19 results in an enzyme that is very sensitive to O_2 and inactivates rapidly, even if just 1% O_2 is introduced during H_2 oxidation. Although some ready state is formed, most of the recoverable activity is restored only upon application of strongly reducing conditions, and a fraction is not recoverable even after 10 h at very negative potential; meanwhile, the EPR spectroscopy at 80 K suggests that the exposure to O_2 results in additional species other than Ni-A and Ni-B. Replacing both C19 and C120 with glycines, in an attempt to mimic the proximal cluster environment of standard [NiFe]-hydrogenases, results in an enzyme that behaves like C19G: after prolonged O_2 exposure during H_2 oxidation, no ready state is recovered upon O_2 removal, but considerable slow reactivation occurs when more reducing conditions (more negative than −250 mV) are applied. As with C19G, the EPR at 80 K suggests that species other than Ni-A and Ni-B are formed. No EPR signal at $g = 4.3$ is observed at 15 K, and thus it is unlikely that Fe has been released, for example through Fe-S cluster degradation. All variants become more O_2-tolerant as the potential is lowered, as shown in Figure 3; this applies particularly to C120G, perhaps reflecting its slightly lower E_{switch} value, for which the lower potential could compensate. In order to address whether reciprocal Gly-to-Cys substitutions could convey an improvement in O_2 tolerance to the normally O_2-sensitive Hyd-2 enzyme, we successfully introduced the necessary point mutations into the gene encoding the Hyd-2 β-subunit on the *E. coli* chromosome. However, we were unable to isolate enzyme from these new strains, and it must be concluded that the Gly-to-Cys substitutions resulted in severely destabilized variant enzymes.

In the O_2-tolerant *Aa* Hase I, the appearance of a complex signal at high potential has been interpreted as arising from spin coupling between the active-site Ni species, the oxidized medial $[3Fe\text{-}4S]^+$ cluster, and the proximal [4Fe-4S] cluster in the 3+ oxidation state. It is therefore proposed that, in addition to the standard $[4Fe\text{-}4S]^{+/2+}$ transition that takes place at lower potential, the proximal cluster undergoes a further one-electron oxidation at high potential.[21] Our results are consistent with this assignment. First, and in agreement with studies on *Re*-MBH,[19] substitution of *both* supernumerary cysteines at the proximal cluster with glycine (C19G/C120G) removes the additional high-potential transition. Second, the high-potential paramagnetic species observed for native Hyd-1 couples with the active-site Ni as well as with the medial [3Fe-4S] cluster, locating the additional paramagnet at the proximal cluster.[21,34,51] The logical mechanistic extension of this assignment is that a key factor in O_2 tolerance is the ability of the proximal cluster to deliver, *immediately*, a further electron to the active site when O_2 attacks.[18,20] The ability to produce the two singularly substituted cysteine-to-glycine variants in *E. coli* now enables deconvolution of the individual contributions made by C19 and C120. The C120G variant, which exhibits considerable O_2 tolerance, displays only low-intensity wings in its EPR spectrum, even at +387 mV. The lack of features (besides the prominent $[3Fe\text{-}4S]^+$ signal) suggests, initially, that an oxidized paramagnetic proximal species is no longer easily formed. However, a more plausible alternative is that its magnetic coupling to nearby paramagnets has been altered due to the oxidized product having a different conformation or spin state. The highly O_2-sensitive C19G variant shows a complex spectrum (developing between +145 and +384 mV) that integrates to two spins per molecule of enzyme and must result also from a paramagnetic center located between the medial cluster and the active site. Therefore, our observations preclude any straightforward link between this signal and O_2 tolerance.

Our results emphasize the need to reconsider the tacit association of kinetically (electrochemically) defined unready species and the spectroscopically defined Ni-A.[8] In EPR sample preparations, Ni-B is formed exclusively after anaerobic inactivation, and this fits perfectly with the PFE kinetic results, which show exclusive or nearly exclusive production of ready, i.e., Ni-B = ready. When we consider the reactions of C19G and C19G/C120G with O_2, the PFE kinetics show that most of the recoverable product should be classed as unready, yet the EPR reveals that very little Ni-A is produced under conditions that most closely match the electrochemistry. We conclude that there is no strong correlation between the EPR-detectable Ni-A and *all* unready species. This has already been noted for the [NiFeSe]-hydrogenase from *Desulfomicrobium baculatum*, which also reacts with O_2 to produce an inactive state that requires a low potential for activation but is not the spectroscopically established Ni-A.[26] Our results lend further support for the formation of inactive states that are thermodynamically more stable than Ni(III)-based species—prime candidates being oxygenated cysteine species[27,28] that may be difficult to observe or distinguish spectroscopically but show up as additional electron density in crystallography.[12,27,52,53]

Having established that C19 is an essential residue for O_2 tolerance, some comment is required regarding the role of C120. First, strain ML24 (encoding the C120G substitution) reproducibly gave yields of hydrogenase that were 2−3 times lower than for strains FTH004, ML23, and ML25. In the case of *Re*-MBH, the C120G exchange prevented growth of *R. eutropha* on H_2 in the presence of O_2, suggesting a problem with assembly in that organism.[19] In that case, the dedicated Fe-S assembly machinery that is required would also need to be functional under aerobic conditions. The increased ratio of ready-to-unready obtained for C19G compared to C19G/C120G under very long O_2 exposure times (Figures 4 and 5) suggests that C120 plays a role in long-term protection, perhaps by stabilizing the proximal cluster.

We are now able to comment on our earlier statements (1)−(6) concerning O_2-tolerant respiratory hydrogenases:

(1) Oxygen tolerance correlates strongly with the ability to maximize formation of the Ni-B (ready) state when O_2 attacks.

(2) A hydrogenase can be very O_2-sensitive, even if it interacts only weakly with CO.

(3) The observation that O_2-tolerant hydrogenases are very poor H_2 producers and have an overpotential requirement for H_2 oxidation is not connected with the presence of supernumerary cysteines at the proximal Fe-S cluster—the O_2 tolerance of an enzyme can be removed without any effect on the catalytic bias or overpotential.

(4) A hydrogenase may be very O_2-sensitive, even if it has a high value for E_{switch}. Note, however, that a high value of E_{switch} (which relates to the ease of reducing Ni-B) remains important for O_2 tolerance because Ni-B must be reactivated rapidly under mildly reducing conditions.
(5) There is no clear correlation between O_2 tolerance and a multiline EPR spectrum that develops at high potentials.
(6) From a chemical viewpoint, O_2 tolerance of an isolated [NiFe]-hydrogenase does not require an additional *pair* of cysteines adjacent to the proximal cluster; one of these conserved cysteines (C19) is far more important for O_2 tolerance than the other (C120).

The question remains as to how the crucial residue C19 confers O_2 tolerance on the enzyme. Viewed in terms of the model for O_2 tolerance,[22] all evidence points to its role being to enhance the transfer of electrons back to the active site when O_2 attacks. However, as stated above, the hypothesis that it confers additional electron-discharging capacity on the proximal cluster is too simplistic, not least because a [4Fe-4S] cluster's ability to perform multiple redox transitions demands some unusual plasticity of the cluster and its environment. Like native Hyd-1, the C19G variant also shows an additional one-electron oxidation at the proximal cluster yet is highly O_2-sensitive, whereas such an oxidation is difficult to detect for C120G, despite this variant retaining considerable O_2 tolerance. Aside from the possibility that this lack of visibility is due to altered spin coupling in C120G, reactive oxygen species are sufficiently powerful oxidants that they can even draw an electron from a site that oxidizes only at a high potential.[52,53] Therefore, just the *availability*, within tunneling distance, of an electron source that can be oxidized and re-reduced rapidly and nonsacrificially could suffice. The O_2 tolerance of C120G would thus arise because the enzyme could still deliver more than one electron rapidly, albeit at a potential that is much higher than accessed in the EPR titration experiments. Without this ability, more electrons must be transferred back from the other Fe-S clusters in the relay. Thus, alternatively (but not exclusively), the presence of C19 might increase the *rate* of immediate response to O_2 attack, perhaps by modifying the proximal cluster to lower its reorganization energy or by improving the electron coupling with the active site. A similar proposal regarding the importance of electron-transfer rates has been made by Liebgott et al.[39] to explain the increase in O_2 tolerance provided when valine-74 of *Df* Hase is replaced by cysteine. Such improved electron-transfer capability could have little effect on H_2 oxidation rates because different rate-determining steps are involved. It is interesting that, in these O_2-tolerant hydrogenases, electron transfer *toward* the active site is used as a defense against O_2 rather than the evolution of H_2.

■ ASSOCIATED CONTENT

Supporting Information. Construction of variants via site-directed mutagenesis, protein purification (Figure S1), anaerobic potential step control experiments (Figure S2), typical inactivation protocols (Figure S3), the effect of CO level on catalytic activity of Hyd-2, native Hyd-1 and variants (Figure S4), CW EPR spectra of H_2-reduced native Hyd-1 and variants at 15 K (Figure S5), wide sweep EPR spectra of the C19G/C120G variant following anaerobic and aerobic inactivation (Figure S6), and complete list of authors for refs 35 and 37. This material is available free of charge via the Internet at http://pubs.acs.org.

■ AUTHOR INFORMATION

Corresponding Author
fraser.armstrong@chem.ox.ac.uk

■ ACKNOWLEDGMENT

We thank Elena Nomerotskaia for invaluable technical assistance throughout the studies and Prof. Michael Haumann for advice and determination of Fe/Ni ratios. We are grateful to Dr. Luet L. Wong for use of UV−visible spectroscopic facilities and Dr. Jeffrey Harmer for helpful advice with EPR. This research was supported by Biological and Biotechnological Sciences Research Council (Grant H003878-1) and Engineering and Physical Sciences Research Council (Grant EP/D044855D/1, supporting the Oxford Centre for Advanced Electron Spin Resonance (CAESR)). A.P. thanks Merton College, Oxford, for a Junior Research Fellowship.

■ REFERENCES

(1) Vignais, P. M.; Billoud, B. *Chem. Rev.* **2007**, *107*, 4206.
(2) Friedrich, B.; Fritsch, J.; Lenz, O. *Curr. Opin. Biotechnol.* **2011**, *22*, 358.
(3) Ghirardi, M. L.; Posewitz, M. C.; Maness, P.-C.; Dubini, A.; Yu, J.; Seibert, M. *Annu. Rev. Plant Biol.* **2007**, *58*, 71.
(4) Reisner, E.; Powell, D. J.; Cavazza, C.; Fontecilla-Camps, J. C.; Armstrong, F. A. *J. Am. Chem. Soc.* **2009**, *131*, 18457.
(5) Wait, A. F.; Parkin, A.; Morley, G. M.; dos Santos, L.; Armstrong, F. A. *J. Phys. Chem. C* **2010**, *114*, 12003.
(6) Tard, C.; Pickett, C. J. *Chem. Rev.* **2009**, *109*, 2245.
(7) Fontecilla-Camps, J. C.; Volbeda, A.; Cavazza, C.; Nicolet, Y. *Chem. Rev.* **2007**, *107*, 4273.
(8) Lamle, S. E.; Albracht, S. P. J.; Armstrong, F. A. *J. Am. Chem. Soc.* **2004**, *126*, 14899.
(9) Liebgott, P.-P.; Dementin, S.; Léger, C.; Rousset, M. *Energy Environ. Sci.* **2011**, *4*, 33.
(10) Vincent, K. A.; Parkin, A.; Armstrong, F. A. *Chem. Rev.* **2007**, *107*, 4366.
(11) Vincent, K. A.; Parkin, A.; Lenz, O.; Albracht, S. P. J.; Fontecilla-Camps, J. C.; Cammack, R.; Friedrich, B.; Armstrong, F. A. *J. Am. Chem. Soc.* **2005**, *127*, 18179.
(12) Volbeda, A.; Martin, L.; Cavazza, C.; Matho, M.; Faber, B. W.; Roseboom, W.; Albracht, S. P. J.; Garcin, E.; Rousset, M.; Fontecilla-Camps, J. C. *J. Biol. Inorg. Chem.* **2005**, *10*, 239.
(13) Cracknell, J. A.; Vincent, K. A.; Ludwig, M.; Lenz, O.; Friedrich, B.; Armstrong, F. A. *J. Am. Chem. Soc.* **2007**, *130*, 424.
(14) Lenz, O.; Ludwig, M.; Schubert, T.; Bürstel, I.; Ganskow, S.; Goris, T.; Schwarze, A.; Friedrich, B. *ChemPhysChem* **2010**, *11*, 1107.
(15) Lukey, M. J.; Parkin, A.; Roessler, M. M.; Murphy, B. J.; Harmer, J.; Palmer, T.; Sargent, F.; Armstrong, F. A. *J. Biol. Chem.* **2010**, *285*, 3928.
(16) Guiral, M.; Tron, P.; Belle, V.; Aubert, C.; Léger, C.; Guigliarelli, B.; Giudici-Orticoni, M.-T. *Int. J. Hydrogen Energy* **2006**, *31*, 1424.
(17) Pandelia, M.-E.; Fourmond, V.; Tron-Infossi, P.; Lojou, E.; Bertrand, P.; Léger, C.; Giudici-Orticoni, M.-T.; Lubitz, W. *J. Am. Chem. Soc.* **2010**, *132*, 6991.
(18) Parkin, A.; Bowman, L.; Roessler, M. M.; Davies, R. A.; Palmer, T.; Armstrong, F. A.; Sargent, F. *FEBS Lett.* **2011**in press.
(19) Goris, T.; Wait, A. F.; Saggu, M.; Fritsch, J.; Heidary, N.; Stein, M.; Zebger, I.; Lendzian, F.; Armstrong, F. A.; Friedrich, B.; Lenz, O. *Nat. Chem. Biol.* **2011**, *7*, 310.
(20) Pandelia, M.-E.; Infossi, P.; Giudici-Orticoni, M.-T.; Lubitz, W. *Biochemistry* **2010**, *49*, 8873.
(21) Pandelia, M.-E.; Nitschke, W.; Infossi, P.; Giudici-Orticoni, M.-T.; Bill, E.; Lubitz, W. *Proc. Natl. Acad. Sci. U.S.A.* **2011**, *108*, 6097.

(22) Cracknell, J. A.; Wait, A. F.; Lenz, O.; Friedrich, B.; Armstrong, F. A. *Proc. Natl. Acad. Sci. U.S.A.* **2009**, *106*, 20681.
(23) Lamle, S. E.; Albracht, S. P. J.; Armstrong, F. A. *J. Am. Chem. Soc.* **2005**, *127*, 6595.
(24) Lubitz, W.; Reijerse, E.; van Gastel, M. *Chem. Rev.* **2007**, *107*, 4331.
(25) De Lacey, A. L.; Fernandez, V. M.; Rousset, M.; Cammack, R. *Chem. Rev.* **2007**, *107*, 4304.
(26) Parkin, A.; Goldet, G.; Cavazza, C.; Fontecilla-Camps, J. C.; Armstrong, F. A. *J. Am. Chem. Soc.* **2008**, *130*, 13410.
(27) Marques, M. C.; Coelho, R.; De Lacey, A. L.; Pereira, I. A. C.; Matias, P. M. *J. Mol. Biol.* **2010**, *396*, 893.
(28) Darensbourg, M. Y.; Weigand, W. *Eur. J. Inorg. Chem.* **2011**, *2011*, 994.
(29) Ogata, H.; Hirota, S.; Nakahara, A.; Komori, H.; Shibata, N.; Kato, T.; Kano, K.; Higuchi, Y. *Structure* **2005**, *13*, 1635.
(30) Vincent, K. A.; Cracknell, J. A.; Lenz, O.; Zebger, I.; Friedrich, B.; Armstrong, F. A. *Proc. Natl. Acad. Sci. U.S.A.* **2005**, *102*, 16951.
(31) Fourmond, V.; Infossi, P.; Giudici-Orticoni, M.-T.; Bertrand, P.; Léger, C. *J. Am. Chem. Soc.* **2010**, *132*, 4848.
(32) Ni_r-SI is a catalytically inactive state and currently thought to contain Ni in the 2+ oxidation state with an OH ligand bound at the bridging position.
(33) Jones, A. K.; Lamle, S. E.; Pershad, H. R.; Vincent, K. A.; Albracht, S. P. J.; Armstrong, F. A. *J. Am. Chem. Soc.* **2003**, *125*, 8505.
(34) Saggu, M.; Zebger, I.; Ludwig, M.; Lenz, O.; Friedrich, B.; Hildebrandt, P.; Lendzian, F. *J. Biol. Chem.* **2009**, *284*, 16264.
(35) Dementin, S.; et al. *J. Am. Chem. Soc.* **2009**, *131*, 10156.
(36) Leroux, F.; Dementin, S.; Burlat, B.; Cournac, L.; Volbeda, A.; Champ, S.; Martin, L.; Guigliarelli, B.; Bertrand, P.; Fontecilla-Camps, J. C.; Rousset, M.; Léger, C. *Proc. Natl. Acad. Sci. U.S.A.* **2008**, *105*, 11188.
(37) Liebgott, P.-P.; et al. *Nat. Chem. Biol.* **2010**, *6*, 63.
(38) Ludwig, M.; Cracknell, J. A.; Vincent, K. A.; Armstrong, F. A.; Lenz, O. *J. Biol. Chem.* **2009**, *284*, 465.
(39) Liebgott, P.-P.; De Lacey, A. L.; Burlat, B.; Cournac, L.; Richaud, P.; Brugna, M.; Fernandez, V. M.; Guigliarelli, B.; Rousset, M.; Léger, C.; Dementin, S. *J. Am. Chem. Soc.* **2011**, *133*, 986.
(40) Fritsch, J.; Löscher, S.; Sanganas, O.; Siebert, E.; Zebger, I.; Stein, M.; Ludwig, M.; De Lacey, A.; Dau, H.; Friedrich, B. R.; Lenz, O.; Haumann, M. *Biochemistry* **2011**, *50*, 5858.
(41) Bard, A. J.; Faulkner, L. R. *Electrochemical Methods*; Wiley: New York, 2001.
(42) Cammack, R. In *Hydrogen as a fuel: Learning from nature*; Cammack, R., Frey, M., Robson, R., Eds.; CRC Press: Boca Raton, FL, 2001; p 73.
(43) Ballantine, S. P.; Boxer, D. H. *J. Bacteriol.* **1985**, *163*, 454.
(44) Bradford, M. M. *Anal. Biochem.* **1976**, *72*, 248.
(45) Dutton, P. L. *Methods Enzymol.* **1978**, *54*, 411.
(46) Stoll, S.; Schweiger, A. *J. Magn. Reson.* **2006**, *178*, 42.
(47) Dubini, A.; Pye, R. L.; Jack, R. L.; Palmer, T.; Sargent, F. *Int. J. Hydrogen Energy* **2002**, *27*, 1413.
(48) Casadaban, M. J.; Cohen, S. N. *Proc. Natl. Acad. Sci. U.S.A.* **1979**, *76*, 4530.
(49) Kurkin, S.; George, S. J.; Thorneley, R. N. F.; Albracht, S. P. J. *Biochemistry* **2004**, *43*, 6820.
(50) Spin integrations were carried out on as-isolated samples reduced using sodium dithionite in the presence of mediators (data not shown). They do not refer to the low-potential H_2-reduced sample, the spectrum of which is shown in Figure S5. Spectra resulting from H_2-reduced samples and dithionite-reduced samples at the same potential are almost superimposable.
(51) Saggu, M.; Teutloff, C.; Ludwig, M.; Brecht, M.; Pandelia, M.-E.; Lenz, O.; Friedrich, B.; Lubitz, W.; Hildebrandt, P.; Lendzian, F.; Bittl, R. *Phys. Chem. Chem. Phys.* **2010**, *12*, 2139.
(52) Yankovskaya, V.; Horsefield, R.; Tornroth, S.; Luna-Chavez, C.; Miyoshi, H.; Léger, C.; Byrne, B.; Cecchini, G.; Iwata, S. *Science* **2003**, *299*, 700.
(53) Atkins, P.; Overton, T.; Rourke, J.; Weller, M.; Armstrong, F. *Shriver and Atkins' Inorganic Chemistry*; Oxford University Press: Oxford, UK, 2010.